Scanning Microscopy

Volume 1996
Number 10 *The Science of Biological Specimen Preparation for Microscopy*
Article 26

12-31-1996

Immunocytochemistry by Electron Spectroscopic Imaging Using Well Defined Boronated Monovalent Antibody Fragments

M. M. Kessels
Max-Planck-Institut für experimentelle Endokrinologie

B. Qualmann
Max-Planck-Institut für experimentelle Endokrinologie

W. D. Sierralta
Max-Planck-Institut für experimentelle Endokrinologie, 106002.547@compuserve.com

Scanning Microscopy Supplement 10, 1996 (pages 327-344) 0892-953X/96$5.00+.25
Scanning Microscopy International, Chicago (AMF O'Hare), IL 60666 USA

IMMUNOCYTOCHEMISTRY BY ELECTRON SPECTROSCOPIC IMAGING USING WELL DEFINED BORONATED MONOVALENT ANTIBODY FRAGMENTS

M.M. Kessels, B. Qualmann and W.D. Sierralta*

Max-Planck-Institut für experimentelle Endokrinologie, Hannover, FRG

(Received for publication June 11, 1996, and in revised form December 31, 1996)

Abstract

Contributing to the rapidly developing field of immunoelectron microscopy a new kind of markers has been created. The element boron, incorporated as very stable carborane clusters into different kinds of peptides, served as a marker detectable by electron spectroscopic imaging (ESI) - an electron microscopic technique with high-resolution potential.

Covalently linked immunoreagents conspicuous by the small size of both antigen recognizing part and marker moiety are accessible by using peptide concepts for label construction and their conjugation with Fab' fragments. Due to a specific labeling of the free thiol groups of the Fab' fragments, the antigen binding capacity was not affected by the attachment of the markers and the resulting immunoprobes exhibited an elongated shape with the antigen combining site and the label located at opposite ends. The labeling densities observed with these reagents were found to be significantly higher than those obtained by using conventional colloidal gold methods.

Combined with digital image processing and analysis systems, boron-based ESI proved to be a powerful approach in ultrastructural immunocytochemistry employing pre- and post-embedding methods.

Key Words: Immunocytochemistry, electron spectroscopic imaging, boron, immunoglobulin fragments, peptides, small sized markers, carboranes, antigen localization, electron energy loss spectroscopy, energy-filtered transmission electron microscopy.

*Address for correspondence
W.D. Sierralta
Max-Planck-Institut für experimentelle Endokrinologie
Postfach 610309
D-30603 Hannover, FRG
Telephone/FAX Number: +49 (511) 5359-156
E-mail: 106002.547@compuserve.com

Introduction

The ultrastructural study of events and functions in biological specimens provides a better comprehension of their cell biology. For this reason, efforts are continuously being made to improve the spatial resolution of the techniques used in electron microscopy for the analysis of biological systems. The improvements in immunoelectron microscopy since the introduction of ferritin as an electron dense label for immunoreagents (Singer, 1959) illustrate the steady search for optimal probes of high resolving power. The application of colloidal gold particles as labels for immunoelectron microscopy (Faulk and Taylor, 1971) increased dramatically the resolution, specificities and resolving power attainable in immunocytochemistry. Although the current immunogold labeled reagents are ideal for routine applications, their relatively large overall size does not support their use if higher resolution is needed as in the tagging of vicinal domains in single macromolecules or of subunits in oligomeric complexes. Another disadvantage of colloidal gold-labeled immunoreagents is the negative charge carried by the particles, causing electrostatic repulsions with components of the specimen and resulting in lower labeling efficiency than expected (van de Plas and Leunissen, 1993).

In order to improve the performance of the electron dense labels, several groups have produced ultrasmall markers. Tetramercury (Lipka *et al.*, 1979), tetrairidium (Furuya *et al.*, 1988), undecagold (Hainfeld, 1987) and tungstate clusters (Keana and Ogan, 1986) have been described and may be covalently bound to immunoglobulins or their fragments. These compounds differ in charge and are in part not stable under the electron beam. All of them are virtually undetectable in conventional transmission electron microscopy, restricting their application to studies of periodical structures with the help of image averaging and processing. Only the 1.4 nm gold cluster developed by Hainfeld and Furuya (1992) has been successfully applied in immunocytochemistry. Post-incubation size-enlargement by coating with metallic silver ("silver-enhancement") (Holgate *et al.*, 1983; Danscher and Nørgaard, 1983) allows for its easy visualization in transmission electron

microscopes and even in light microscopes.

All the labels described above belong to a group that may be detected in transmission electron microscopes because elements with a high atomic number strongly scatter elastically electrons of the beam. The probability and strength of this elastic Rutherford scattering, based on the deflection of beam electrons by the positively charged atomic nucleus, strongly depend upon the sample thickness and the atomic number of the elements present.

A different approach is used in the ultrastructural detection of specific elements by their inelastic scattering properties via electron spectroscopic imaging (ESI) and electron energy loss spectroscopy (EELS) (Ottensmeyer, 1982; 1984; Colliex, 1986; Reimer, 1991). Here, irradiated electrons interact with the shell electrons of the sample, and - by transferring energy - cause excitation or even ionization of the specimen atoms. A part of the electrons in the transmitted beam has therefore lost a defined amount of energy, which allows to draw conclusions about the kind and state of the atoms present in the specimen. To split the electrons according to their energy content, the transmission electron microscopes must be equipped with energy filters (Castaing and Henry, 1962; Henkelman and Ottensmeyer, 1974): The electrons leaving the specimen are deflected on circular paths by the Lorentz force of a magnetic field; the deflection radii are proportional to the energy content of the electrons.

An electron energy loss spectrum represents graphically the intensity distribution of electrons according to their energy content. The presence of an element occurring in sufficient quantities in a specimen can be demonstrated on the basis of its specific absorption edge. The positions of these absorption edges correspond to the characteristic binding and therefore ionization energies of a specific element according to the energy level (K-shell, L-shell etc.). These edges are superimposed on the offset of an intense, broad peak (plasmon peak) which includes electrons having created collective excitations, inter- and intraband transitions. For this reason, the spectrum or the elemental map must be cleared from the relatively large amount of the non-element-specific, intense background to obtain a netto element signal.

The representation of the spatial distribution of electrons of a specific selected energy loss in the form of two-dimensional images is called electron spectroscopic imaging. To obtain the net elemental distribution for a chosen element it is necessary to record, in addition to the element-specific picture just above the absorption edge, at least one reference image below the edge onset. This permits the extrapolation of the non-element-specific background.

Energy filtered transmission electron microscopic (EFTEM) methods have been rapidly developing into very powerful tools for elemental microanalysis in biological specimens during the last years. Although mainly used for detections of naturally occurring (Ottensmeyer and Andrew, 1980; Arsenault and Ottensmeyer, 1983; Leapman and Andrews, 1991) or exogenously supplied elements (Köpf-Maier and Martin, 1989; Wagner and Chen, 1990) - often as precipitates - these techniques may also be used in immunocytochemistry to detect reagents labeled with appropriate marker molecules. Outstanding features of this method are the high spatial resolution and sensitivity potentials achievable. In commercial instruments, ESI allows for a spatial resolution of 0.5 nm and provides enough sensitivity to detect 50 accumulated atoms of a light element like phosphorus (Adamson-Sharpe and Ottensmeyer, 1981).

Marker molecules for ESI-immunocytochemistry must fulfill the following requirements: The elemental marker should not be a component of the investigated cells or tissues and should exhibit a strong, sharp absorption edge in the electron energy loss spectrum sufficiently distinct from those of other elements present. Furthermore, the detection limit must be exceeded, ensured by a high topical density of the element chosen.

Organo-boron compounds appear to be particularly well suited for an application as labels in ESI-based immunocytochemistry. Beside its absence in most biological specimens and its sharp absorption edge in EELS not particularly overlapping with those of other elements normally present, boron has the property to form stable and defined covalent clusters which can be incorporated into organic molecules (Plešek, 1992; Hawthorne, 1993; Morin, 1995).

In 1989, a first experiment with boron-labeled immunoreagents was described by Bendayan *et al.* (1989). They employed a heterogeneous, positively charged marker with varying boron content, a boronated polylysine (Barth *et al.*, 1986; Alam *et al.*, 1989) linked to protein A, for the indirect detection of antigenic sites. Their approach resulted in strong ESI signals, with a reduced spatial resolution, limited by the relatively large size of the probe (approximately 15 nm - not considering the sizes of the primary reagents used in the indirect approach). These immunoreagents did not allow for high resolution analyses with ESI, compelling compact, small-sized marker molecules. A size-reduction should additionally increase tagging efficiencies, because steric hindrances are lowered and infiltrations of section's surface depths are facilitated (Horisberger, 1981; Yokota, 1988).

A direct boronation of antibodies through multiple attachment of small, boron-containing molecules (Mizusawa *et al.*, 1982; Alam *et al.*, 1985) is limited

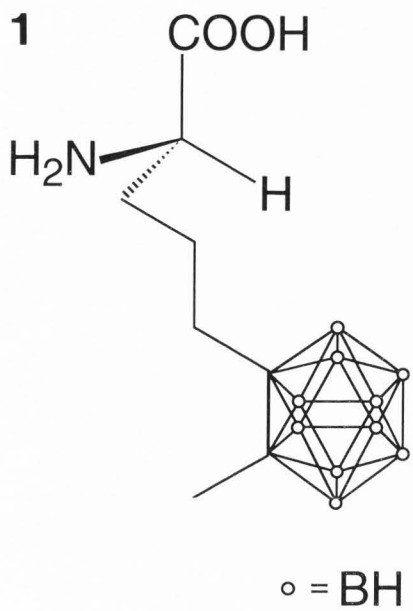

Figure 1. Stereochemical structure of the carborane cluster containing amino acid used for the different peptide syntheses. L-5-(2-methyl-1,2-dicarba-closo-dodecaborane(12)-1-yl-)2-amino pentanoic acid (L-MeCBA **1**) was produced by the bislactim ether method (Schöllkopf *et al.*, 1981) following the concept of auxilliars, i.e., a glycine building block is incorporated into a molecule containing a group which sterically controls the alkylation leading enantioselectively to the desired amino acid derivative.

---

because of the strong effects on immunoreactivity and solubility of the proteins. Therefore, research was recently more focussed on the grafting of boron-loaded polymers to single sites of carrier molecules. However, the difficulties caused in this procedure by the inherent heterogeneity of the boron-containing labels like poly-lysine (Barth *et al.*, 1986; 1989), poly-ornithine (Tamat *et al.*, 1989), dextranes (Abraham *et al.*, 1989; Pettersson *et al.*, 1989) and starburst dendrimers (Barth *et al.*, 1994) have stimulated the design and synthesis of more defined molecules, such as oligomeric peptides containing carboranyl amino acids (Varadarajan and Hawthorne, 1991; Kane *et al.*, 1993; Leusch *et al.*, 1994).

Development of Probes for EFTEM

Immunocytochemistry by electron spectroscopic imaging requires the development of appropriate immunoreagents consisting of a small and homogeneous marker moiety and an efficient antigen recognizing part. In this context the use of Fab' fragments of antibodies is advantageous due to their small size amounting to 5 nm x 4 nm x 3 nm (Hainfeld, 1987). These fragments are able to reach even antigenic sites of which the accessibility is diminished by other constituents of the specimen or by the tertiary structure of the given target protein, they easily penetrate the depths of the section surface and can also be used as valuable reagents for pre-embedding methods. Since the dimensions of the antibody fragments are quite low, the achievable lateral resolution is high. The Fab' fragments exhibit one single antigen combining site, i.e., they are monovalent, a basic requirement for examinations of some special problems.

Additionally, Fab' fragments provide the possibility of a regiospecific derivatization with the marker molecule, since the thiol groups of the former hinge region of the IgG (immunoglobulin G) molecule are accessible and allow for a SH-specific labeling at a domain opposite to the antigen combining site (Kato *et al.*, 1976; Yoshitake *et al.*, 1982; Padlan, 1994). Thus, the immunoreactivity is not affected by the marker compound. This is in strong contrast to labeling approaches using all the electron-rich moieties of the protein for covalent linkages.

In the design of the marker molecules the following special demands must be satisfied:

[1] a fully accessible, reactive handle permitting the thiol-selective conjugation to the antibody fragment has to be incorporated,

[2] the marker molecule should carry a high boron load spread over a minimized volume to exceed the ESI detection limit and to achieve a high signal to noise ratio,

[3] the label should be homogeneous in structure, boron content and size,

[4] a fluorescent group should be incorporated to quantify the conjugation reaction,

[5] the compound has to be soluble in a solvent miscible with water or even in water itself.

Since using amino acids as well characterized multifunctional building blocks is an appropriate approach, we applied peptide chemistry to fulfill these requirements.

First of all, an amino acid containing the element boron was necessary. R,S-5-(2-methyl-1,2-dicarba-closo-dodecaborane(12)-1-yl-)2-amino pentanoic acid (D,L-MeCBA) (Varadarajan and Hawthorne, 1991) is an attractive compound for our application, since 10 boron atoms are condensed in a cluster of high stability and steric hindrances are comparatively low. This carboranyl amino acid has been successfully used in peptide syntheses for different purposes (Varadarajan and Hawthorne, 1991; Kane *et al.*, 1993; Leusch *et al.*, 1994).

First experiences with linear racemic peptides

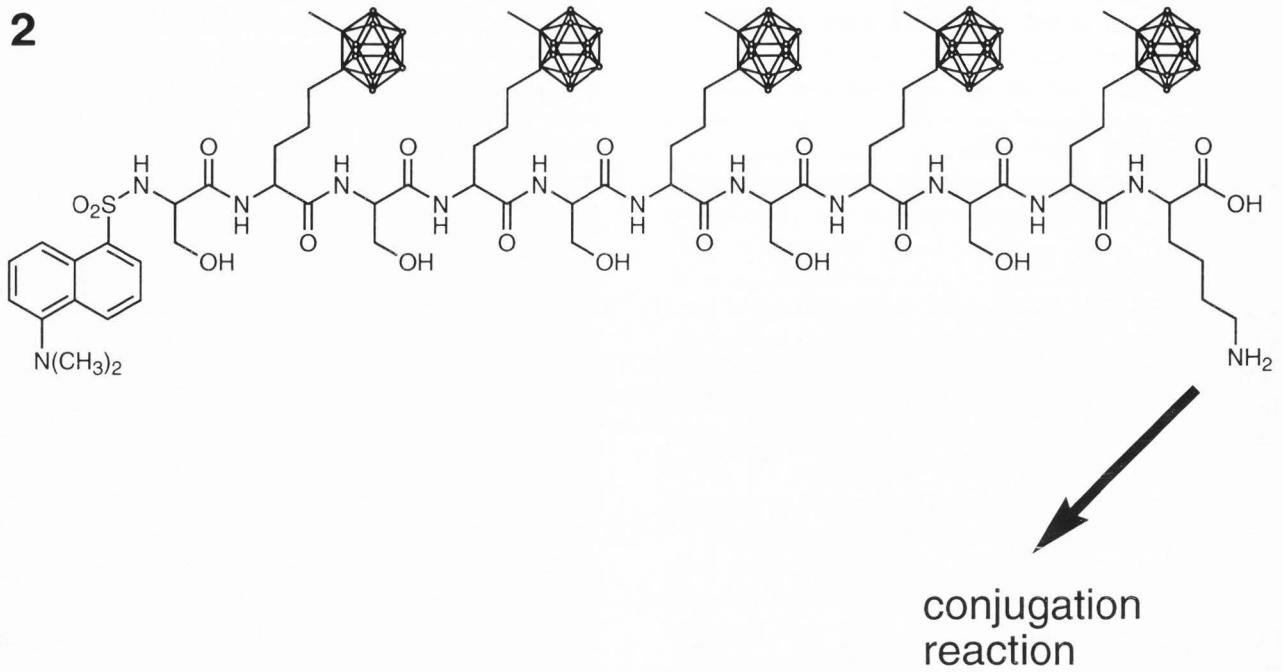

Figure 2. Structure of the linear, N-terminally dansylated peptide **2** consisting of 11 amino acids (5 MeCBAs **1**, 5 serines and a lysine), which has been successfully linked to Fab' antibody fragments and detected by ESI using the incorporated boron as marker element.

(Leusch *et al.*, 1994) encouraged us to work on the further development of boron-rich marker molecules. Two routes were followed to improve the performance of the peptides: Since an enantioselective synthesis allows for a more defined and condensed secondary structure of the marker, we developed an efficient synthesis of the pure L-enantiomer of the carborane-containing amino acid MeCBA **1** (Fig. 1). The synthesis is short, convenient and proceeds in high overall yield (68%). The carboranyl amino acid MeCBA **1** is obtainable in high enantiomeric purity (enantiomeric excess > 98%) and in amounts sufficient for peptide syntheses (Kessels and Qualmann, 1996). The second way to enhance the signals of the marker molecules consists in the incorporation of a greater number of carboranyl amino acids.

The linear peptides produced followed partly the concept of Varadarajan and Hawthorne (1991). They contain a dansyl group as a fluorescence marker, a lysine moiety as the later coupling site and a different number of MeCBAs. Diverging from Varadarajan and Hawthorne (1991), alternating serines were incorporated to improve the solubility of the marker peptides and a segment condensation synthesis in solution was used (Leusch *et al.*, 1994; Kessels, 1996; Kessels *et al.*, 1996). In general, the extremely high hydrophobicity of the carborane cage often represents a problem; the side chain of carboranylalanine, for example, is reported to be 1000 times more hydrophobic than that of valine (Fauchère *et al.*, 1980). To decrease the hydrophobicity of the compounds we incorporated polar groups like hydroxyl and amino functions.

The all-L-peptide **2** produced (Fig. 2) represents a small and compact marker molecule. The maximal possible length extension assuming a fully stretched conformation is approximately 3.5 nm. The possibility of forming a more condensed secondary structure in solution ought to be considered, especially in the case of enantiomerically pure compounds.

The peptide proved to be soluble in polar organic solvents like dimethylformamide and different alcohols and in aqueous organic mixtures allowing for coupling to the antibody fragments Fab'. Conjugations were performed with heterobifunctional crosslinkers of the N-hydroxysuccinimidylmaleimidyl type linking the free thiol groups of Fab' with the amino group of the lysine anchor present in the marker peptide (Kessels *et al.*, 1996). The efficiency of conjugation exhibited a strong dependence on the length of the spacer moiety incorporated in the different crosslinkers used (Kessels, 1996), probably due to steric hindrances. The coupling reactions were verified by fluorescence examination. The boron content of the peptide **2**-immunoprobes was impressively demonstrated by electron energy loss spec-

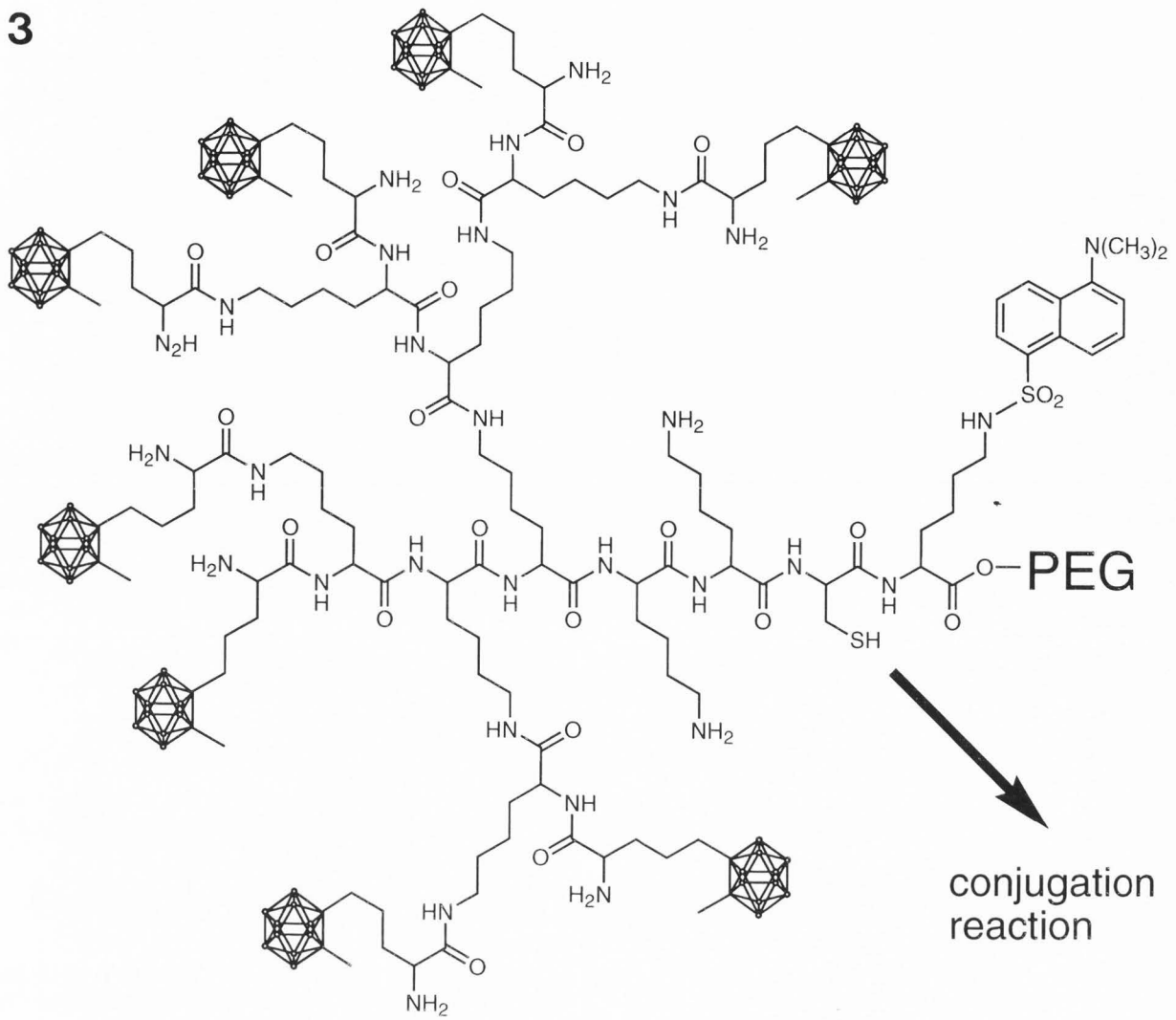

Figure 3. Molecular structure of the dendritic peptide construct **3** containing 8 carboranyl amino acids attached at the outer surface of a poly(α,ϵ-L-lysine) core and a linear tail carrying the coupling site for Fab' conjugation, the dansyl group and a polyethylene glycol chain (PEG) spaced from the dendrimer moiety by 2 lysines. An identical peptide, only lacking the PEG-tail, was also produced. The peptides **2** (Fig. 2) and **3** are shown in the same size.

---

troscopy (Kessels *et al.*, 1996).

A further synthesized elongated peptide (8 incorporated carboranyl amino acids, 21 steps) exhibited a poor solubility in aqueous organic mixtures and the coupling ratios were low (Kessels, 1996). These immunoreagents were not promising - obviously a limitation of the linear peptide concept had been reached.

Furthermore, there are some common disadvantages of the linear peptide syntheses, such as the very laborious, multi-step procedures (even though we used a segment condensation approach) leading to low overall yields (even assuming, e.g., a yield of 90% in each individual step the overall yield of a 15-step synthesis (peptide **2**) would nevertheless be only 20% and that of a 21-step procedure only 11%, respectively). Another disadvantage is the necessary, time-consuming and increasingly difficult characterization of each synthetic intermediate by analytical means like thin layer chromatography, nuclear magnetic resonance spectroscopy and mass spectrometry.

To bypass the limitation and the inconveniences we left the linear approach and generated spherical dendritic peptides carrying the carboranyl amino acids at the outer surface (Qualmann *et al.*, 1996b). We developed a solid phase peptide synthesis (SPPS; Merrifield, 1963) employing the orthogonal concept of fluorenyl-methyl-oxycarbonyl-SPPS (Atherton *et al.*, 1981). The coupling difficulties encountered in solid phase and solution

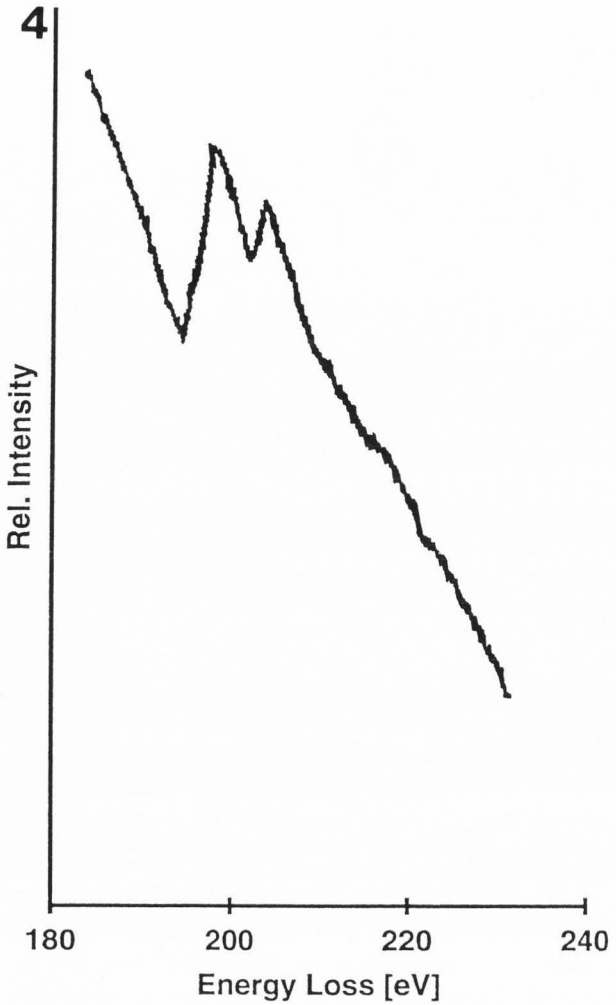

Figure 4. Schematic presentation of the different functional moieties incorporated into the dendritic peptide **3** and their arrangement.

---

synthesis of carboranyl amino acid-containing oligopeptides derive from steric hindrances particularly of the N-terminus of the carboranyl amino acids due to the bulky carborane moiety (Varadarajan and Hawthorne, 1991; Kane *et al.*, 1993; Leusch *et al.*, 1994). The attachment of the carboranyl amino acids to the terminal amino groups of a poly(α,ϵ-L-lysine) dendrimer (Denkewalter and Kolc, 1981; Tam, 1988) in a final acylation step overcame these limitations. The amino functions of the molecule, whose quantity grows exponentially with each step of the dendrimer synthesis, are spherically distributed, thus steric hindrances are diminished and acylation occurs quantitatively (Posnett *et al.*, 1988; Qualmann *et al.*, 1996b).

Due to the globular shape of the marker molecules the topical boron concentration is very high. The maxi-

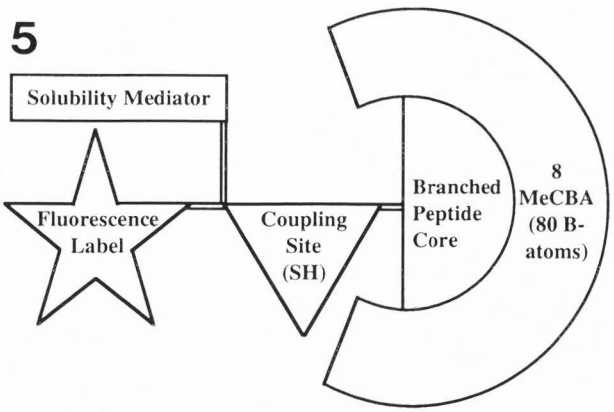

Figure 5. Electron energy loss spectrum of immunoreagents bearing peptide **3** adsorbed to nitrocellulose-coated gold grids. Notice the sharp boron K-shell absorption edge at 196 eV rising from the steep declining background curve. Instrument settings: objective aperture 90 μm, spectrometer entrance aperture 100 μm, slit width 1-2 eV, beam current 30 μA, magnification 30000x, scan speed 1.6 eVs^{-1}.

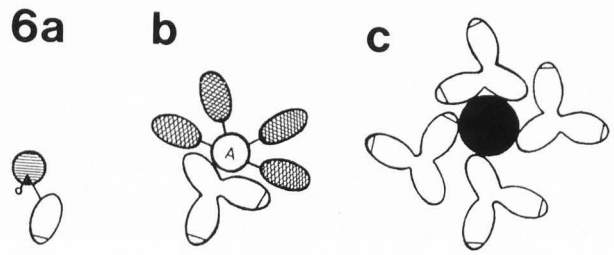

Figure 6. Comparison of sizes and shapes of different immunoreagents. Schematic representations. **a**. Fab' fragment conjugated with the boronated dendritic peptide **3**. **b**. Indirect immunoprobe employed by Bendayan *et al.* (1989), i.e., an antibody detected by protein A, which has been linked with several boronated polylysines. **c**. Conventional colloidal gold (Au_{6nm}) immunoreagent.

Figure 7 (*on facing page*). Comparison of conventional immunogold technique with boron electron spectroscopic imaging. **a**, **b**. Labeling of the secretory vesicles (sv) in somatotrophic cells of porcine anterior pituitary with goat anti-GH, detected by rabbit anti goat-Au_{10nm}. *N* nucleus, *arrow* plasma membrane with adjacent non-somatotroph. **c**. ESI with anti-GH-Fab'-peptide-**2**-conjugate: one of the two background images taken below the boron absorption edge (*178 eV*), an image just above the boron absorption edge (*201 eV*), a conventional zero loss image (*0 eV*) and the net boron distribution (*B-distribution*) calculated by the three-window method (150 eV, 178 eV, 201 eV). With kind permission from Kessels *et al.* (1996), Fig. 3; © Springer Verlag, Heidelberg, FRG.

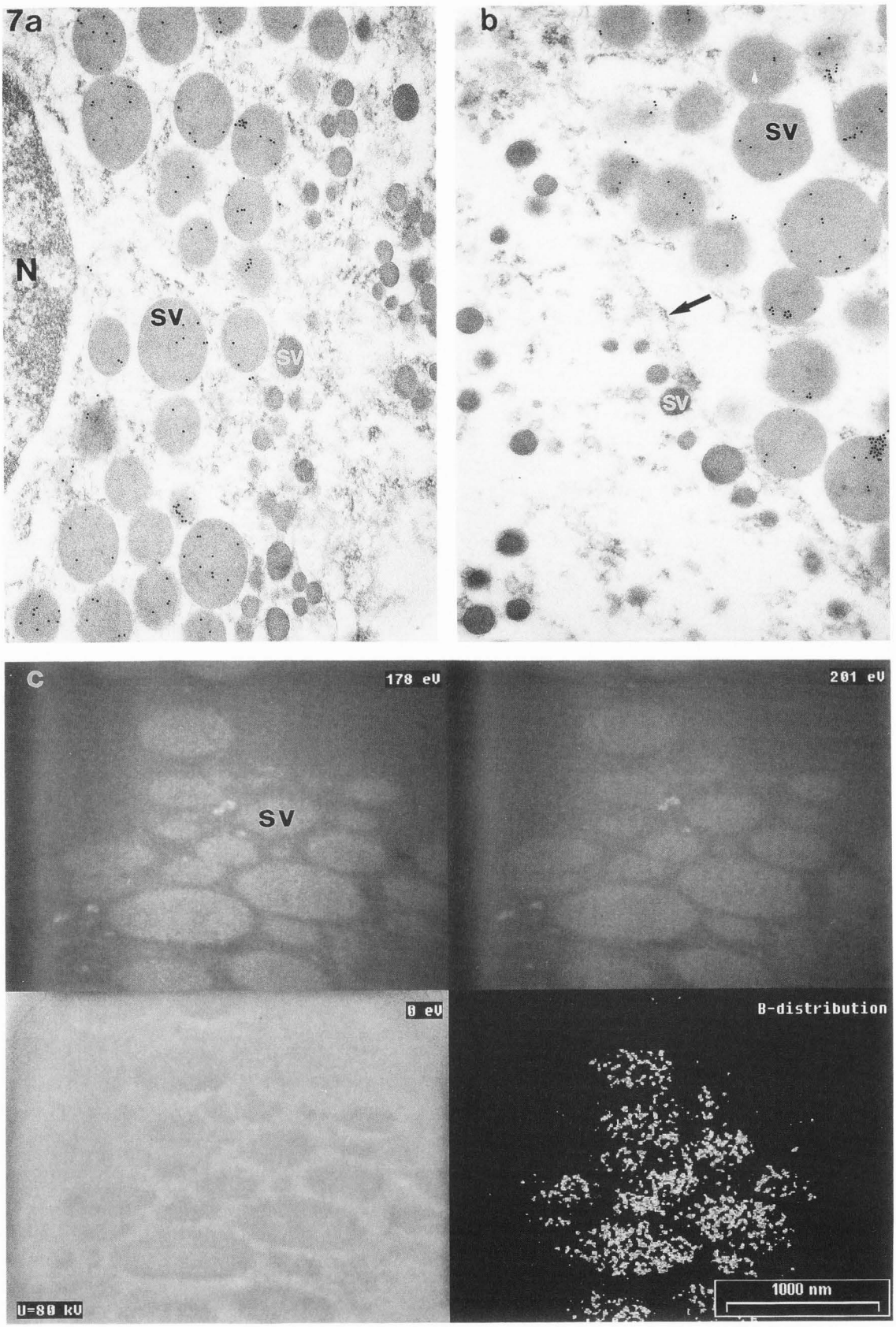
7a
N
SV
SV
b
SV
SV
C
178 eV
SV
201 eV
0 eV
B-distribution
1000 nm
U=80 kV

mal extension of the 80 boron atoms can theoretically reach 4 nm. In fact, for a poly(α,ϵ-L-lysine) dendrimer of the same size terminally acylated with a further generation of lysines instead of carboranyl amino acids a diameter of 2.28 nm in solution is described (Aharoni *et al.*, 1981).

The marker peptides prepared consist of two parts (Fig. 3): the globular, branched core of lysines with 8 terminal amino groups each carrying a carboranyl amino acid - the marker moiety - and a C-terminal, linear peptide chain containing the coupling site (a thiol function of an incorporated cysteine) and a fluorescence label (a dansylated lysine like in the linear peptides) both spaced from the voluminous hepta(α,ϵ-L-lysine) core by two more lysines. Their highly polar amino functions should also enhance the hydrophilicity of the molecule.

A further increase of the hydrophilicity was obtained by the derivatisation of the C-terminus with a polyethyleneglycol (PEG) tail. This solubility mediator proved to be necessary since the marker peptide lacking the polyether tail was only poorly soluble in aqueous solutions. Probably due to its low solubility the conjugation efficiency was as low as that observed for the elongated linear peptide containing 8 carboranyl amino acids. In contrast, the PEG-bearing analog **3** (Figs. 3 and 4) exhibited good solubilities in a wide variety of solvents (e.g., chloroform, methanol, water) and reacted smoothly in Fab'-conjugations with different types of crosslinkers employed (Qualmann *et al.*, 1996a,b). No disturbing precipitates were formed and the associated loss of antibodies was diminished, ensuring the use of even monoclonal antibody fragments usually available in only moderate quantities (Parham, 1983). Furthermore, the addition of organic solvents to dissolve the marker peptide can be omitted reducing the risk of decreasing the antigen binding capacity of the Fab' molecules.

The quality of the immunoprobes was again checked by fluorescence measurements and examinations using an energy filtered transmission electron microscope to detect the marker element boron. An electron energy loss spectrum of an immunoreagent bearing the marker peptide **3** is shown in Fig. 5 exhibiting the sharp boron absorption edge at an energy loss of 196 eV.

The marker compound was proven to be remarkably stable during beam irradiation: no losses of signal intensity in successively recorded electron energy loss spectra were detected when a given area of the specimen was exposed to a 30 μA electron beam for more than five minutes (Qualmann *et al.*, 1996a). This is in striking contrast to observations of Huxham *et al.* (1992). They examined borate adsorbed to polystyrene beads and described a rapid loss of boron signals: in their case after only 3 minutes of exposure a complete loss of signals was seen. In contrast, immunoprobes containing boron in the form of chemically and thermically very stable and covalently attached closo-carborane cages (Wade, 1976) are not affected by irradiation, thus proving to be appropriate for immunocytochemistry.

(*Figure 8 on facing page*)

Figure 8. Uptake of BSA by ileal enterocytes of newborn piglets demonstrated by tagging with the Fab'-boronated peptide conjugate and ESI-examination (three-window-method - 150 eV, 178 eV, 201 eV). Differences in labeling of BSA-containing vesicles obtained with the BSA-specific boronated immunoprobe (a, c) and a non-related control conjugate (b). **a.** Overview consisting of the background images taken below the boron absorption edge (*178 eV*), the boron specific image just above the edge (*201 eV*), the zero loss image (*0 eV*) and the net boron distribution. Labeling performed with anti-BSA-Fab' fragments conjugated with peptide **3**. The sizes and shapes of the vesicles are delineated even by the BSA-tagging alone, permitting the examination of antigen localization just by comparison of the calculated boron distribution and the zero loss image. The frame (in a) marks the part of the vesicle shown beyond in 8fold enlargement (c) The grayscale signal intensities range from white (highest intensity) over light gray to dark gray). **b.** ESI-micrograph demonstrating the background noise detected over a vesicle area in control sections incubated with a boronated anti-GH immunoprobe. The images b and c are shown at the same magnification. With kind permission from Qualmann *et al.* (1996a); © Blackwell Science Ltd, Oxford, UK.

In summary, defined, boron-rich marker peptides of small, homogeneous size were generated in good purity. Since standard procedures of solid phase peptide synthesis are used in the case of the dendritic peptide **3**, the synthesis is reliable, easy to control by the analytical means of SPPS and proceeds in high overall yields.

In general, the immunoreagents are of elongated shape carrying the covalently linked marker at the opposite end of the antigen combining site, thus immunoreactivity is not affected sterically by the marker peptides and the lateral extension of the immunoprobe just depends on the diameter of the Fab' fragment (approximately 4 nm). In contrast, other immunoreagents previously described show much larger spatial extensions: in conventional immunogold labeling the diameter of the colloidal gold is greatly enlarged by the antibody coat and in the boron/ESI method of Bendayan *et al.* (1989) the heterogeneously linear boronated polylysines linked to the protein A, used as indirect label, contribute substantially to the overall size of the marker even assuming a rather globular structure (Figure 6).

All the immunoreagents produced have been puri-

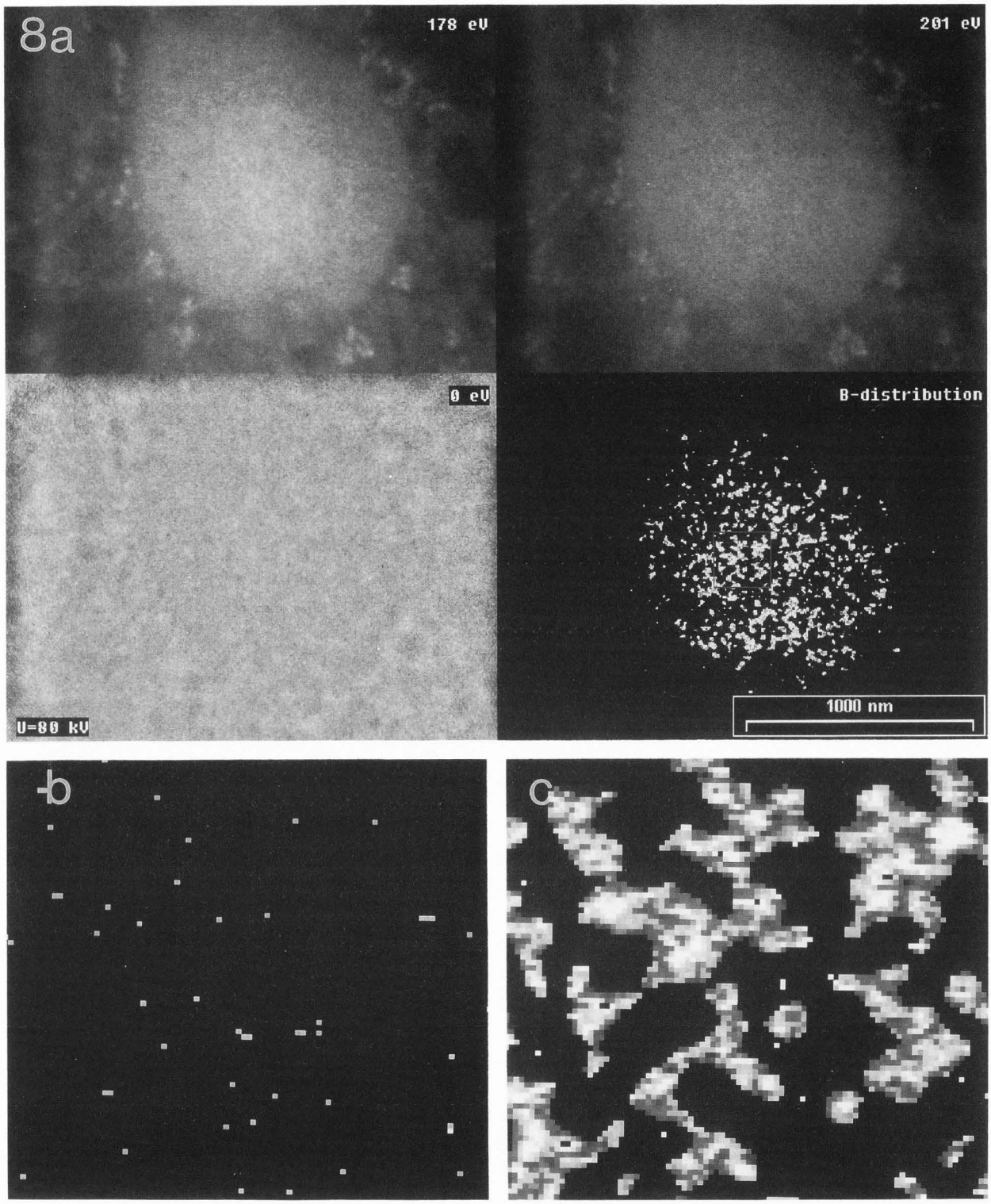

fied from unreacted low molecular weight components of the conjugation reaction, concentrated and stored at 4°C in the presence of 1 mM azide as preservative and 0.5% (w/v) bovine serum albumin and ovalbumin as expander, respectively. No loss in immunoreactivity and no aggregation was observed even during prolonged storage of several months (Kessels *et al.*, 1996; Qualmann *et al.*, 1996a; Qualmann, 1996).

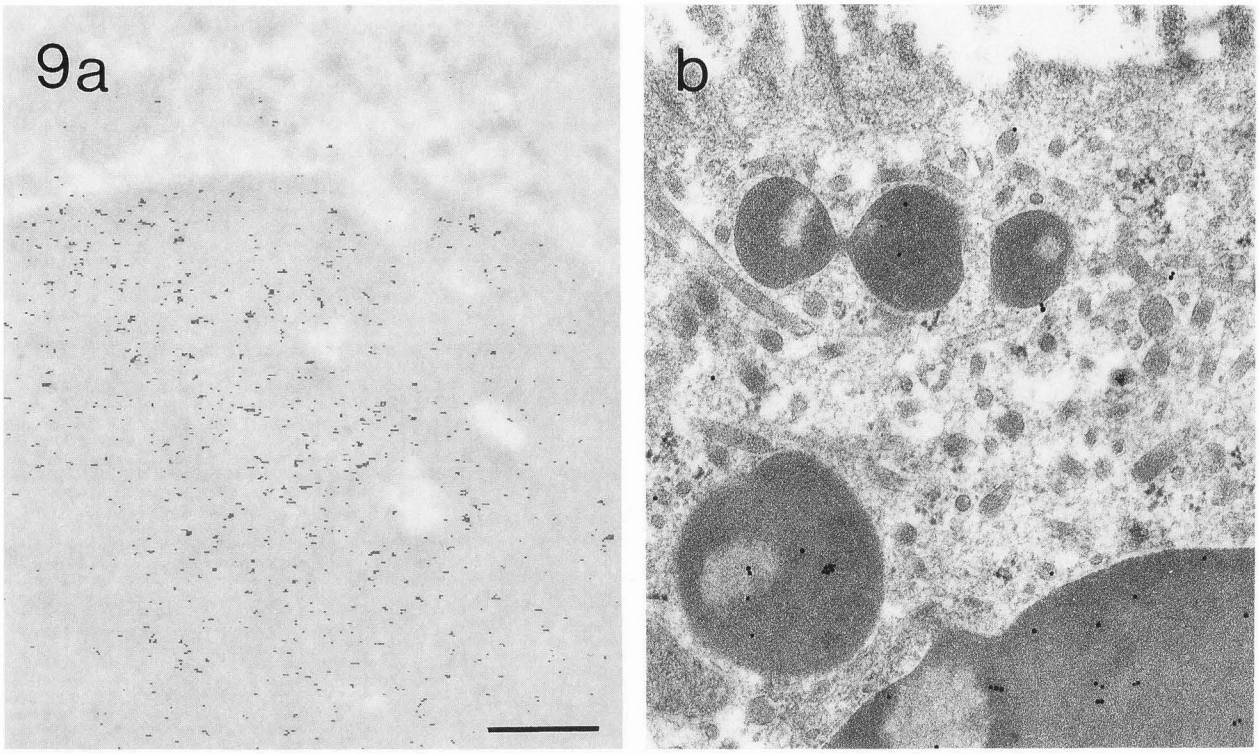

Figure 9. Assignment of BSA-labeling to transcytotic vesicles in an epithelial cell of ileum taken from newborn piglets after the administration of bovine serum. **a.** Superimposition of calculated net boron signals (shown in here in black, but in green in the original publication) obtained by incubation with anti-BSA-Fab'-peptide **3** on the corresponding zero loss image of endocytotic vesicles (unstained, 40 nm thin section). **b.** Conventional direct immunogold labeling ($F(ab')_2$-Au_{12nm}) of BSA in endocytotic vesicles of different size. Section (80 nm) contrasted with OsO_4, uranyl acetate and lead citrate. Scale bar: 400 nm. With kind permission from Qualmann *et al.* (1996a); © Blackwell Science Ltd, Oxford, UK.

Requirements in the Preparation of Specimens for Immunocytochemistry

Retention of antigenicity in sufficient amounts for good antigen-antibody interactions requires mild fixation. The choice of embedding resin also has a great influence on the analysis by immunocytochemistry, especially if post-embedding is performed. The suitability of Epon for pre-embedding experiments and of Lowicryl-embedded tissue for post-embedding immunocytochemistry with ESI has been reported by Bendayan *et al.* (1989). For our studies with boron-labeled antibody fragments, Spurr resin (Spurr, 1969) was found suitable even for post-embedding ESI immunocytochemistry because sections of this plastic allows for the reaction of antigens at the depths of the surface with immunoreagents as confirmed by conventional immunogold labeling. As shown in the Figures 7, 9 and 10, a satisfactory retention in antigenicity after fixation, dehydration and embedding procedures was secured.

The resin showed practically no interference with the detection of boron; the high purity of the plastic components, free of traces of elements like sulphur and phosphorus, resulted in a very low background (see Figure 10, for example).

A crucial factor in the performance of energy-filtered transmission electron microscopic methods is the thickness of the sample, because the probability of multiple scattering events decreasing the signal to noise ratio augments with the thickness of the probe under the electron beam. The energy loss of an electron is only specific for an element if it is attributed to a single scattering event in the specimen. Therefore, if the percentage of multiple scattering events should not exceed 15%, the samples should be no thicker than about 0.3 mean free paths for total electron scatter; this means a thickness of about 30 nm for sections of biological material (Ottensmeyer, 1986). Despite their thinness, these sections of polymerized Spurr resin exhibited reasonable stability under the electron beam with low tendency to tear or to drift. Sections of material embedded in Spurr resin stay adherent on 600 mesh-

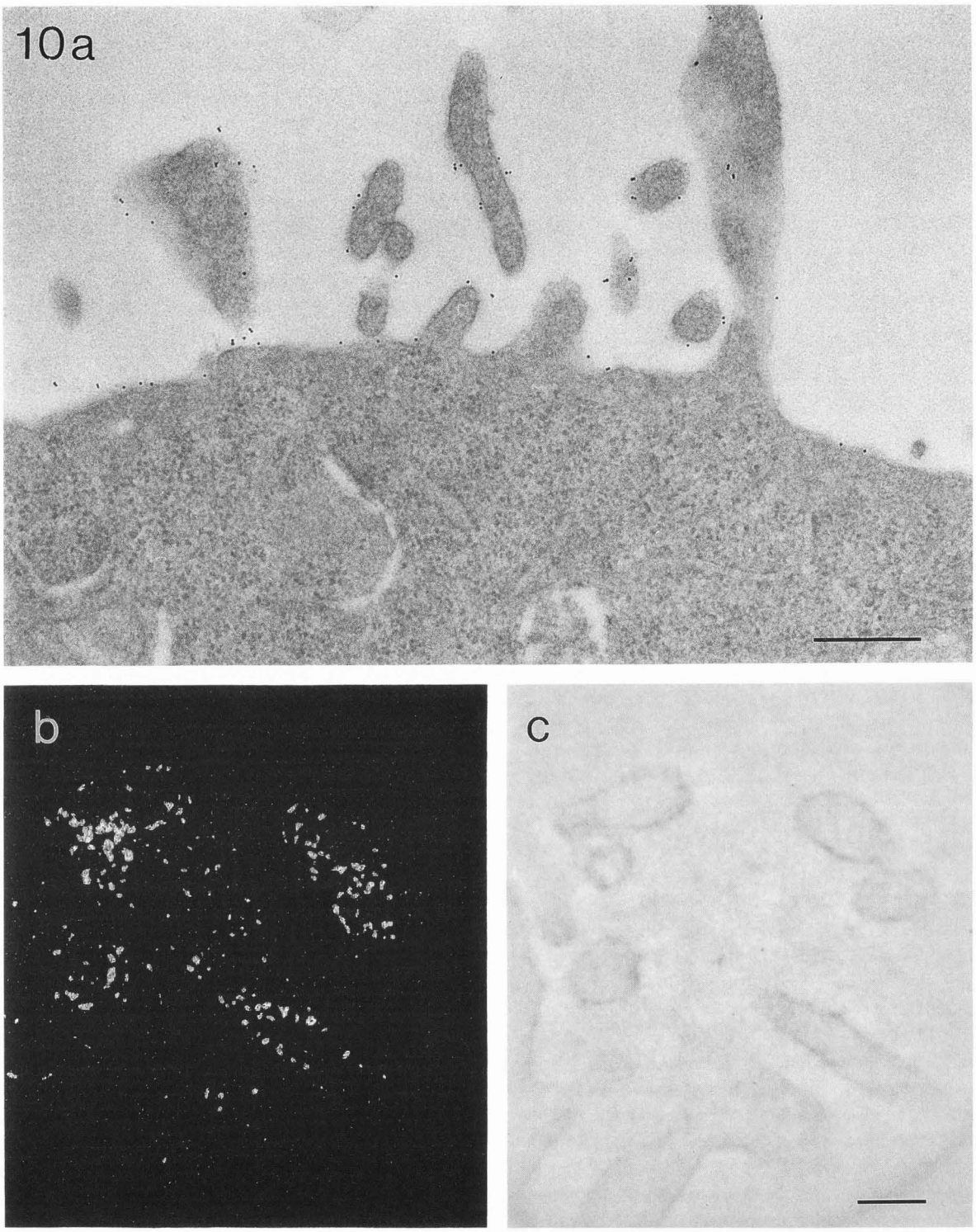

Figure 10. Labelling of high affinity IgE receptors on membranes of rat basophilic leukemia cells (line RBL-2H3, cells were incubated with the immunoreagent at 4°C in the presence of azide to prevent internalization). **a.** Immunogold labelling using 6 nm gold coated with rat monoclonal antibody J17 (contrasted 100 nm section). **b.** Grayscale representation of the net boron distribution in an ultrathin section of cells incubated with a boron-containing immunoconjugate of J17. **c.** Zero-loss image corresponding to the area shown in **b**. Scale bars: 400 nm (**a**), 150 nm (**b,c**).

grids allowing incubations on aqueous solutions and avoiding supporting films which will undesiredly increase the path length of beam electrons through the specimen. An increase in stability may be obtained by subsequent carbon coating, but this significantly lowers the signal to noise ratio.

Additionally, contrasting of the sections with OsO_4, uranyl acetate, lead citrate or other heavy metal stains should be omitted otherwise a reduction of the element-specific signal is obtained.

Hardware Requirements for ESI-Immunocytochemistry

In order to detect specific elements by electron spectroscopic imaging, the microscopes have to be upgraded with an imaging electron spectrometer. Two different types of arrangements of energy filters have been realized in transmission electron microscopes commercially available at present:

[1] the addition of a post-column spectrometer to a conventional transmission electron microscope (cTEM) as accessory,

[2] the integration of an in-column spectrometer in the magnification system of specially constructed TEMs.

The work described here was carried out with a ZEISS 902 (Zeiss, Oberkochen, FRG), which is equipped with an imaging spectrometer of the prism-mirror-prism type (Castaing and Henry, 1962) and an energy selecting slit. Electron energy loss spectra were recorded with the electron detector of the microscope connected to a digital compensation X/Y-plotter. The effective diameter of the selected area analyzed is restricted by the spectrometer entrance aperture and the magnification.

In ultrathin sections, only a relatively small portion of electrons is inelastically scattered (approx. 1.5%; Ottensmeyer, 1982) because the ionization cross section is very small even for elements with a low atomic number. Therefore, EFTEM techniques require greater electron doses than usual, which may result in radiation damage, instabilities and even mass losses in the specimen. If the acceleration voltage is raised, the impulse- and thus the energy-transfer during interaction with matter is lower, in consequence, the mean free path length increases. The signal to noise ratio augments, because the probability of multiple scattering events is diminished. In the ZEISS 902, the acceleration voltage is factory-limited to 80 kV to prevent the electrical collapse of the filter. For operations at higher voltage, the electrostatic mirror must be replaced by a fully magnetic deflection system, as realized in the ZEISS 912 with an omega filter (Zanchi *et al.*, 1975) design.

The efficient collection of the scattered electrons is of uppermost importance in order to keep the total exposure time and thus radiation-induced alterations in the specimen under the electron beam low. A large objective aperture allows the capture of scattered electrons in a great area.

Fundamental limitations of the photographic materials, like their relatively low sensitivity and non-linear responses as well as the tedious chemical development have stimulated the search of appropriate alternative recording systems in electron microscopy (Krivanek and Mooney, 1993; De Ruijter, 1995). The fast development of electronic media in the last years has been of considerable benefit for ESI. Thus, the detection of the low level of electrons inelastically scattered by the lighter elements present in the specimen makes the use of electronic cameras in almost all the cases mandatory.

Besides a high sensitivity, the high-quality electronic cameras currently in use possess a good spatial resolution, with less or no geometric distortion, are able to acquire the images fast, react to changes in the input intensity rapidly and last, but not least give signal outputs proportional to the incoming energy currents.

Two sorts of electronic cameras are currently in use: the silicon intensified target (SIT) vidicon cameras and the solid-state slow-scan charge-coupled devices (SCCD). In the first type, a scintillator on top of the electronic tube transduces the electrons into photons and a photoconductive layer under the scintillator changes its resistance in proportion to the total number of photons absorbed. An electron beam produced inside the tube scans the faceplate and produces an interlaced analogue signal compatible with video processor devices, like monitors, frame grabbers, recorders.

In the SCCD, discrete microscopic wells are built on a chip, each well representing a pixel. The wells accumulate charge in proportion to the photons collected. After a given time, the electrons accumulated in a row of pixels are shifted to an on-chip output amplifier. The charge accumulated in the chip is read out by the orderly transference of all rows. As in the case of vidicon tubes, the SCCD-analogue images are further amplified and digitized by separate electronics, resulting in images with pixel intensities expressed in digital numbers, allowing an uncomplicated processing (Center for Light Microscopic Imaging and Biotechnology, CLMIB, 1995).

The SCCD have many advantages over the SIT cameras, especially as far as sensitivity, resolution, speed, noise, response time and uniformity are concerned. Of uppermost importance is the low level of "shading" (nonuniformity in the camera, especially in the corners of the image scanned) that SCCD exhibit as compared to the SIT cameras. Probably the major advantage of the SIT camera is its lower price.

Great success in the recording and analysis of element-specific images in EFTEM has been achieved by the application of digital image analysis. Recording times of a few seconds when information is digitalized and integrated contrast sharply with exposure times of up to 100 seconds needed for photographic film material. Computer assistance is an essential component in data acquisition, data processing and displaying of results.

To obtain net elemental maps, the relatively strong background signal has to be removed. The photographically recording and subtraction of elemental maps can be done by either the rather imprecise, subjective and less reproducible photographic approach or by employing an image processor. The computer-assisted use of two or more reference images and the application of different kinds of complex algorithms allows to extrapolate the background signal underneath the ionization edge with great accuracy. For the calculation of the boron net distribution on sections of material from biological specimens embedded in resin, we employed a three-window-method. From two images recorded at energy losses of 150 eV and 178 eV (width of the energy selecting slit was approx. 15 eV) below the boron K-edge, the best fitting parameters for the background model curve are examined for each of the 765 x 574 pixel and extrapolated for the third image recorded at 201 eV above the edge; the difference between the extrapolated background curve and the recorded data at an energy loss of 201 eV represents the net element signal. Our microscope is upgraded with a Dage SIT camera and connected to the Image Analysis System ESI Vision from AnalySIS, Münster (FRG). The newer version (2.1) of this analysis program will additionally permit the use of multi-window methods for background calculation.

Immunocytochemical Applications

The validity of the new approach has been proven by labeling different antigens employing either pre- or post-embedding methods. A first set of experiments was performed using polyclonal goat antibodies directed against porcine growth hormone (GH). Fab' fragments prepared from them were labeled with the boronated peptides and employed for a direct post-embedding detection of the antigen in ultrathin sections of porcine pituitary embedded in Spurr resin.

The pituitary gland contains different kinds of secretory cells, which can be distinguished by examining their morphology. Somatotrophs stand out for their large and rather low electron dense secretory vesicles filling wide areas of the cytoplasm. Conventional immunogold labeling was performed using anti-goat IgG-Au_{10nm} as secondary antibody to examine the subcellular distribution of the growth hormone. The labeling was practically restricted to secretory vesicles of somatotrophs (Fig. 7); other parts of the cells like cytoplasm and nuclei were not labeled. Secretory vesicles containing hormones other than GH exhibited no gold tags either.

As the antigen GH occurs in large amounts in these organelles, this system served as an excellent biological system to allow the reliable development of the ESI-immunocytochemical approach based on the newly created boron-rich marker molecules. Since high accuracy is desired, we used the three-window-method for our ESI examinations. Fig. 7c shows the GH-localization by means of ESI-immunocytochemistry, an example of the labeling using the linear peptide **2** as marker is shown. Similar results were obtained using peptide **3** conjugates (Kessels, 1996). The net distribution of the marker element boron was assessed by recording images below and just above the boron edge. The higher brightness of the presented 178 eV background image compared to the 201 eV image reflects the steep declining of the recorded intensities at higher energy losses out of which the boron edge is rising as it can be observed in the detail of an electron energy loss spectrum shown in Fig. 5. Using the three-window method an intense labeling of GH-secretory vesicles was observed. In many cases the signal density was high enough to reveal the size and shape of the tagged organelles. Other constituents of the cells and secretory vesicles of other cell types exhibited no boron signals, demonstrating the specificity of the labeling procedure.

A second experimental model was used to confirm the validity of the approach: the transepithelial passage of proteins from the lumen of the small gut through the ileal enterocytes into the circulation of newborn piglets (Nelson, 1932; Brambell, 1959). We employed the heterologous bovine serum albumin (BSA) as a model protein to follow this process (Sierralta *et al.*, 1994). The system was tested by conventional immunocytochemistry using a direct reagent (12 nm gold coated with $F(ab')_2$ fragments of polyclonal goat antibodies against BSA). Ileal endocytotic vesicles filled with the antigen were observed in the epithelial cells, the vesicles were very heterogeneous in size (Figs. 8 and 9).

The labeling with immunoconjugates bearing boronated peptides **2** and **3**, respectively, analysed by ESI also localized the antigen in the endocytotic vesicles (Figs. 8 and 9; Qualmann, 1996; Qualmann *et al.*, 1996a). Other compartments of the ileal cells exhibited no boron signals. Corresponding to the density of antigens present the sizes and shapes of the vesicles were again delineated even by the net boron signals alone.

A very exact examination of the localization of calculated net boron signals can be performed by superimposing them on the conventional zero-loss image

(Fig. 9a) or on images at other energy losses generally providing a higher contrast of morphological structures (e.g., below the carbon edge at an energy loss of 250 eV). In general, zero-loss images recorded in ESI examinations of ultrathin sections of biological materials display low contrast, due to their thinness, due to the omitted contrasting step and due to the fact that the images are collected with wide objective apertures to ensure an efficient data collection (e.g., we used an objective aperture of 90 μm instead of 60 μm as chosen in standard cTEM applications) leading to very light images which are no longer optimally recorded by the camera. Therefore, for graphical presentations zero-loss images have as a rule to be digitally remastered.

In a subsequent set of experiments the immunoboron approach was extended to pre-embedding methods. High affinity membrane receptors for IgE present on basophils and mast cells (Metzger and Ishizaka, 1982; Kinet, 1989) are able to induce secretions of mediators leading to allergic and inflammatory symptoms. We localized the IgE receptor protein FCϵR I employing the rat basophilic leukemia cell line RBL-2H3 first by conventional immunogold methods. Colloidal gold of 6 nm in diameter coated with the monoclonal rat antibody J17 (Ortega *et al.*, 1988) showed the IgE-receptor protein to be localized under the given conditions at the plasma membrane (Fig. 10a). The antibody is directed against an extracellular domain (Ortega *et al.*, 1988).

These experiments were followed by subcellular examinations based on the immunoreaction with antibody fragments labeled with the boronated peptide **3** (Qualmann, 1996; Kessels, 1996). Boron signals were detected at the surface of the plasma membrane and the extensions of the cells. Due to the high labeling efficiency of the antigen which occurs in approximately 270000 molecules per cell (Mao *et al.*, 1992), the membranes were often drawn by the net boron signals alone (Fig. 10b). Additionally, the ultrathin sections of the pre-embedded material showed very well the low level of interference introduced by Spurr resin in the boron detection by ESI. The background signals recorded in areas of pure resin were low (Fig. 10b).

In all cases several control experiments were run to assess the background noise by omitting the boronated probe or by using boron-labeled antibodies directed against antigens non-occurring in the material under investigation. The results were comparable, unspecific labeling was not observed (see Figure 8b, for example).

The high signal densities obtained were impressively seen independent of the experimental model used. The labeling efficiencies were estimated to be more than one order of magnitude higher than those observed with the immunogold labeling method (Kessels *et al.*, 1996). The very small, boronated immunoreagents we employed thus confirmed the observations of Horisberger (1981) and Yokota (1988), who demonstrated the crucial influence of the spatial extension of immunoreagents on the achievable tagging frequency.

The exploitation of the high-resolving power of ESI using novel marker compounds like those described here, i.e., the full spatial resolution of two or more neighbored or even overlapping marker molecules, will be left to future experiments. Preliminary results show that with our present picture acquisition system a magnification of at least 150000x should be used to obtain pixel areas small enough (approximately 0.5 nm and smaller) to image accurately the intensity distribution of boron signals predicted from the peptide structures, i.e. to display the markers with sufficient precision.

In general, ultrasmall immunoreagents will allow for successful studies on interactions between macromolecular domains and between constituents of supramolecular complexes by means of high-resolution electron microscopy. Since the achievable resolution of ESI is high and can be further enhanced by image analysis systems (Adamson-Sharpe and Ottensmeyer, 1981), immunocytochemistry based on ESI/EELS techniques may become of great importance. Furthermore, immunocytochemistry by ESI-detection benefits from the separation of morphological data and marker localization data opening the gate for multiple immunostaining not distinguished by different sizes of not further characterized electron-dense spots but elementally by ESI-examinations of markers consisting of different marker elements. Using modern digital superimposure techniques electron microscopy will become "colored".

The actual focussing on the use of boron is due to its now well known chemistry (Stock, 1933; Lipscomb, 1977) and appeared very promising since in addition, the study of the distribution and subcellular localization of administered boronated compounds represents an important aspect for boron neutron capture therapy of cancer (Locher, 1936; Barth *et al.*, 1990). Also in this context, the development of modified head groups with even higher boron load and better solubility to be used in our dendritic peptide concept represents a promising project.

Despite the exclusive use of boron so far, this element should not remain the only one being potentially incorporable into immunoprobes; several other elements have been successfully detected by ESI/EELS over the last years (Costa *et al.*, 1978; Jeanguillaume, 1987; Köpf-Maier and Martin, 1989; Wagner and Chen, 1990; Fehrenbach *et al.*, 1994). It will be interesting to see what kind of marker elements will be used next.

Acknowledgements

The authors wish to express their gratitude to Prof. P.W. Jungblut, Max-Planck-Institut für experimentelle Endokrinologie, Hannover, FRG, for his encouragement. We are grateful to Prof. L. Moroder and Mr. H.-J. Musiol, Max-Planck-Institut für Biochemie, Martinsried, FRG, for their invaluable help in peptide construction. We also thank Dr. F. Klobasa, Institut für Tierzucht und Tierverhalten (FAL), Mariensee, FRG, and Prof. I. Pecht, Weizmann Institute of Science, Rehovot, Israel, for the antibodies provided and Mrs. V. Ashe for linguistic assistance.

References

Abraham R, Müller R, Gabel D (1989) Boronated antibodies for neutron capture therapy. Strahlenter Onkol **165**: 148-151.

Adamson-Sharpe KM, Ottensmeyer FP (1981) Spatial resolution and detection sensitivity in microanalysis by electron energy loss selected imaging. J Microsc **122**: 309-314.

Aharoni SM, Crosby III CR, Walsh EK (1982) Size and solution properties of globular tert-butyloxycarbonyl-poly(α,ϵ-L-lysine). Macromolecules **15**: 1093-1098.

Alam F, Soloway AH, McGuire JE, Barth R, Carey WE, Adams DM (1985) Dicesium N-succinimidyl 3-(undecahydro-closo-dodecaboranyldithio)propionate, a novel heterobifunctional boronating agent. J Med Chem **28**: 522-525.

Alam F, Soloway AH, Barth RF, Mafune N, Adams DM, Knoth WH (1989) Boron neutron capture therapy: Linkage of a boronated macromolecule to monoclonal antibodies directed against tumor-associated antigens. J Med Chem **32**: 2326-2330.

Atherton E, Logan CJ, Sheppard RC (1981) Peptide synthesis. Part 2. Procedures for solid phase synthesis using N^{α}-fluorenylmethoxycarbonylanino-acids on polymamide support. Synthesis of substance P and of acyl carrier protein 65-74 decapeptide. J Chem Soc Perkin Trans **1**: 538-546.

Arsenault AR, Ottensmeyer FP (1983) Quantitative spatial distributions of calcium, phosphorus, and sulfur in calcifying epiphysis by high resolution electron spectroscopic imaging. Proc Natl Acad Sci USA **80**: 1322-1326.

Barth RF, Alam F, Soloway AH, Adams DM, Steplewski Z (1986) Boronated monoclonal antibody 17-1A for potential neutron capture therapy of colorectal cancer. Hybridoma **5**: S43-S50.

Barth RF, Mafune N, Alam F, Adams DM, Soloway AH, Makroglou GE, Oredipe OA, Blue TE, Steplewski Z (1989) Conjugation, purification and characterization of boronated monoclonal antibodies for use in neutron capture therapy. Strahlenther Onkol **165**: 142-145.

Barth RF, Soloway AH, Fairchild RG (1990) Boron neutron capture therapy of cancer. Cancer Res **50**: 1061-1070.

Barth RF, Adams DM, Soloway AH, Alam F, Daby MV (1994) Boronated starburst dendrimer-monoclonal antibody immunoconjugates: evaluation as a potential delivery system for neutron capture therapy. Bioconjugate Chem **5**: 58-66.

Bendayan M, Barth RF, Gingras D, Londoño I, Robinson PT, Alam F, Adams DM, Mattiazzi L (1989) Electron spectroscopic imaging for high-resolution immunocytochemistry: Use of boronated protein A. J Histochem Cytochem **37**: 573-580.

Brambell FWR (1959) The transmission of immunoglobulins from the mother to the foetal and newborn young. Proc Nutr Sci **23**: 35-41.

Castaing R, Henry L (1962) Filtrage magnetique des vitesses en microscopie electronique. (Magnetic speed filtering in electron microscopy). C R Acad Sci Paris **255**: 76-78.

Center for Light Microscopic Imaging and Biotechnology (CLMIB) (1995) A guide to selecting electronic cameras for light microscope-based imaging. American Laboratory **4**: 25-40.

Colliex C (1986) Electron-energy loss spectroscopy analysis and imaging of biological specimens. Ann N Y Acad Sciences **483**: 311-325.

Costa JL, Joy DC, Maher DM, Kirk KL & Hui SW (1978) Fluorinated molecule as a tracer: Difluoro-serotonin in human platelets mapped by electron energy-loss spectroscopy. Science **200**: 537-539.

Danscher G, Nørgaard JOR (1983) Light microscopic visualization of colloidal gold on resin-embedded tissue. J Histochem Cytochem **31**: 1394-1398.

De Ruijter WJ (1995) Imaging properties and application of slow-scan charge-coupled device cameras suitable for electron microscopy. Micron **26**: 247-275.

Denkewalter RG, Kolc J, Lukasavage WJ; Allied Corp (1981) Macromolecular highly branched homogeneous compound based on lysine units. US-A 428972, Chem Abstr (1985) **102**: 79324q.

Fauchère JL, Kim Quang Do, Jow PYC, Hansch C (1980) Unusually strong lipophilicity of "fat" or "super"amino-acids, including a new reference value for glycine. Experientia **36**: 1203-1204.

Faulk WP, Taylor GM (1971) An immunocolloid method for the electron microscope. Immunochemistry **8**: 1081-1083.

Fehrenbach H, Schmiedl A, Brasch F, Richter J (1994) Evaluation of lanthanide tracer methods in the study of mammalian pulmonary parenchyma and cardiac

muscle by electron spectroscopic imaging. J Microsc **174**: 207-223.

Furuya FR, Miller LL, Hainfeld JF, Christopfel WC, Kenny PW (1988) Use of $Ir_4(CO)_{11}$ to measure the lengths of organic molecules with a scanning transmission electron microscope. J Am Chem Soc **110**: 641-643.

Hainfeld JF (1987) A small gold-conjugated antibody label: improved resolution for electron microscopy. Science **236**: 450-454.

Hainfeld JF, Furuya FR (1992) A 1.4-nm gold cluster covalently attached to antibodies improves immunolabeling. J Histochem Cytochem **40**: 177-184.

Hawthorne MF (1993) Die Rolle der Chemie in der Entwicklung einer Krebstherapie durch die Bor-Neutroneneinfangreaktion. (The role of chemistry in the development of boron neutron capture therapy of cancer) Angew Chem **105**: 997-1033; Also published as: The role of chemistry in the development of boron neutron capture therapy of cancer. Angew Chem Int Ed Engl **32**: 950-984.

Henkelman RM, Ottensmeyer FP (1974) An energy filter for biological electron microscopy. J Microsc **102**: 79-94.

Holgate CS, Jackson P, Cowen PN, Bird CC (1983) Immunogold-silver staining: new method of immunostaining with enhanced sensitivity. J Histochem Cytochem **31**: 938-944.

Horisberger M (1981) Colloidal gold: a cytochemical marker for light and fluorescent microscopy and for transmission and scanning electron microscopy. Scanning Electron Microsc 1981; II: 9-31.

Huxham IM, Gaze MN, Workman P, Mairs RJ (1992) The use of parallel EEL spectral imaging and elemental mapping in the rapid assessment of anti-cancer drug localization. J Microsc **166**: 367-380.

Jeanguillaume C (1987) Electron energy loss spectroscopy and biology. Scanning Microsc **1**: 437-450.

Kane RR, Pak RH, Hawthorne MF (1993) Solution-phase segment synthesis of boron-rich peptides. J Org Chem **58**: 991-992.

Kato K, Fukui H, Hamaguchi Y, Ishikawa E (1976) Enzyme-linked immunoassay: conjugation of the Fab' fragment of rabbit IgG with β-D-galactosidase from *E. coli* and its use for immunoassay. J Immunol **116**: 1554-1560.

Keana JFW, Ogan MD (1986) Functionalized Keggin- and Dawson-type cyclopentadienyltitanium heteropolytungstate anions: small, individually distinguishable labels for conventional transmission electron microscope. 1. Synthesis. J Am Chem Soc **108**: 7951-7957.

Kessels MM (1996) Immuncytochemie auf der Basis von Electron Spectroscopic Imaging. Design, Synthese und Anwendung Bor-haltiger Markermoleküle (Immunocytochemistry based on electron spectroscopic imaging. Design, synthesis, and application of boron-containing marker molecules). Doctoral Thesis, University of Hannover, FRG.

Kessels MM, Qualmann B (1996) Facile enantioselective synthesis of (S)-5-(2-methyl-1,2-dicarba-closo-dodecaborane(12)-1-yl)-2-aminopentanoic acid (L-MeCBA) using the bislactim ether method. J prakt Chem **338**: 89-91.

Kessels MM, Qualmann B, Klobasa F, Sierralta WD (1996) Immunocytochemistry by electron spectroscopic imaging using a homogenous boronated peptide. Cell Tissue Res **284**: 239-245.

Köpf-Maier P, Martin R (1989) Subcellular distribution of titanium in the liver after treatment with the antitumor agent titanocene dichloride. Virch Arch B [Cell. Pathol] **57**, 213-222.

Kinet JP (1989) Antibody-cell interactions: Fc receptors. Cell **57**: 351-354.

Krivanek OL, Mooney PE (1993) Applications of slow-scan CCD cameras in transmission electron microscopy. Ultramicroscopy **49**: 95-108.

Leapman RD, Andrews SB (1991) Biological electron energy loss spectroscopy: The present and the future. Microsc Microanal Microstruct **2**: 387-394.

Leusch A, Jungblut PW, Moroder L (1994) Design and synthesis of carboranyl peptides as carriers of 1,2-dicarbadodecacarborane clusters. Synthesis: 305-308.

Lipka JJ, Lippard SJ, Wall JS (1979) Visualization of polymercurimethane-labeled fd bacteriophage in the scanning transmission electron microscope. Science **206**: 1419-1421.

Lipscomb WN (1977) Die Borane und ihre Derivate - Nobel-Vortrag (The boranes and their derivatives - nobel lecture). Angew Chem **89**: 685-696.

Locher GL (1936) Biological effects and therapeutic possibilities of neutrons. Am J Roentgenol Radium Ther **36**: 1-13.

Mao SY, Pfeiffer JR, Oliver JM, Metzger H (1992) Effects of subunit mutation on the localization to coated pits and internalization of cross-linked IgE-receptor complexes. J Immunol **151**: 2760-2774.

Merrifield RB (1963) Solid phase peptide synthesis. I. The synthesis of a tetrapeptide. J Am Chem Soc **85**: 2149-2154.

Metzger H, Ishizaka T (eds) (1982) Symposium: transmembrane signalling by receptor aggregation: the mast cell receptor for IgE as a case of study. Fed Proc **41**: 7-34.

Mizusawa E, Dahlman HL, Bennett SJ, Goldenberg DM, Hawthorne MF (1982) Neutron-capture therapy of human cancer: In vitro results on the preparation of boron-labeled antibodies to carcinoembryonic antigen.

Proc Natl Acad Sci USA **79**: 3011-3014.

Morin C (1995) The chemistry of boron analogues of biomolecules. Tetrahedron **50**: 12521-12569.

Nelson JB (1932) The maternal transmission of vaccinal immunity in swine. J Exp Med **56**: 835-840.

Ortega E, Schweitzer-Stenner R, Pecht I (1988) Possible orientational constraits determine secretory signals induced by aggregation of IgE receptors on mast cells. EMBO J **7**: 4101-4109.

Ottensmeyer FP (1982) Scattered electrons in microscopy and microanalysis. Science **215**: 461-466.

Ottensmeyer FP (1984) Electron spectroscopic imaging: parallel energy filtering and microanalysis in the fixed-beam electron microscope. J Ultrastruct Res **88**: 121-134.

Ottensmeyer FP (1986) Elemental mapping by energy filtration: advantages, limitations, and compromises. Ann N Y Acad Sci **483**: 339-350.

Ottensmeyer FP, Andrew JW (1980) High-resolution microanalysis of biological specimens by electron energy loss spectroscopy and by electron spectroscopic imaging. J Ultrastruct Res **72**: 336-348.

Padlan EA (1994) Anatomy of the antibody molecule. Molec Immunol **31**: 169-217.

Parham P (1983) On the fragmentation of monoclonal IgG1, IgG2a, and IgG2b from BALB/c mice. J Immunol **131**: 2895-2902.

Pettersson ML, Courel MN, Girard N, Abraham R, Gabel D, Thellier M, Delpech B (1989) Immunoreactivity of boronated antibodies. J Immunol Methods **126**: 95-102.

Plešek J (1992) Potential applications of the boron cluster compounds. Chem Rev **92**: 269-278.

Posnett DN, McGrath H, Tam JP (1988) A novel method for producing anti-peptide antibodies. J Biol Chem **263**: 1719-1725.

Qualmann B (1996) Hochauflösende Methoden der Immunelektronenmikroskopie. Abbildende Elektronen-Energieverlust-Spektroskopie zur Antigendetektion mittels Bor-enthaltender Markermoleküle (High-resolution methods in immunocytochemistry. Electron spectroscopic imaging for antigen detection using boron-containing marker molecules). Doctoral Thesis, University of Hannover, FRG.

Qualmann B, Kessels MM, Klobasa F, Jungblut PW, Sierralta WD (1996a) Electron spectroscopic imaging of antigens by reaction with boronated antibodies. J Microsc **183**: 69-77.

Qualmann B, Kessels MM, Musiol HJ, Sierralta WD, Jungblut PW, Moroder L (1996b) Synthese Borreicher Lysindendrimere zur Proteinmarkierung in der Elektronenmikroskopie (Synthesis of boron-rich lysine dendrimers as protein labels in electron microscopy) Angew Chem **108**: 970-973. Also published as: Synthesis of boron-rich lysine dendrimers as protein labels in electron microscopy. Angew Chem Int Ed Engl **35**: 909-911.

Reimer L (1991) Energy-filtering transmission electron microscopy. In: Advances in Electronics and Electron Physics. Hawkes PW (ed). Academic Press Inc., Boston. **81**: 43-126.

Schöllkopf U, Groth U, Deng C (1981) Enantioselektive Synthese von (R)-Aminosäuren unter Verwendung von L-Valin als chiralem Hilfsstoff (Enantioselective synthesis of (R)-amino acids using L-Valin as chiral agent) Angew Chem **93**: 793-795. Also published as: Enantioselective synthesis of (R)-amino acids using L-Valin as chiral agent. Angew Chem Int Ed Engl **20**: 798-800.

Sierralta WD, Qualmann B, Klobasa F (1994) Passage of a heterologous protein through ileal enterocytes of newborn piglets: Immunolabelling of bovine serum albumin at the light- and electron microscopic level. J Vet Med A **41**: 421-430.

Singer SJ (1959) Preparation of an electron-dense antibody conjugate. Nature **183**: 1523-1524.

Stock A (1933) The Hydrides of Boron and Silicon. Cornell University Press, Ithaca, New York. pp 1-250.

Spurr AR (1969) A low-viscosity epoxy resin embedding medium for electron microscopy. J Ultrastruct Res **26**: 31-43.

Tam JP (1988) Synthetic peptide vaccine design: synthesis and properties of a high-density multiple antigenic peptide system. Proc Natl Acad Sci USA **85**: 5409-5413.

Tamat SR, Patwardhan A, Moore DE, Kabral A, Bradstock K, Hersey P, Allen BJ (1989) Boronated monoclonal antibodies for potential neutron capture therapy of malignant melanoma and leukaemia. Strahlenther Onkol **165**: 145-147.

van de Plas P, Leunissen JLM (1993) Ultrasmall gold probes: characteristics and use in immuno(cyto)chemical studies. In: Antibodies in Cell Biology. Asai DJ (ed). Academic Press, San Diego. pp 241-257.

Varadarajan A, Hawthorne MF (1991) Novel carboranyl amino acids and peptides: Reagents for antibody modification and subsequent neutron-capture studies. Bioconjugate Chem **2**: 242-253.

Wade K (1976) Structural and bonding patterns in cluster chemistry. Adv Inorg Radiochem **18**: 1-66.

Wagner RC, Chen SC (1990) Ultrastructural distribution of terbium across capillary endothelium: detection by electron spectroscopic imaging and electron energy loss spectroscopy. J Histochem Cytochem **38**: 275-282.

Yokota S (1988) Effect of particle size on labeling density for catalase in protein A-gold immunocytochem-

istry. J Histochem Cytochem **36**: 107-109.

Yoshitake S, Imagawa M, Ishikwa E, Nijtsu Y, Urushizaki I, Nishiura M, Kanazawa R, Kurosaki H, Tachibana S, Nakazawa N, Ogawa H (1982) Mild and efficient conjugation of rabbit Fab' and horseradish peroxidase using a maleimide compound and its use for enzyme immunoassay. J Biochem **92**: 1413-1424.

Zanchi G, Perez JP, Sevely J (1975) Adaption of a magnetic filtering device on a one megavolt electron microscope. Optik **43**: 495-501.

Discussion with Reviewers

F.P. Ottensmeyer: An improvement I would urge is in the presentation, or perhaps even in the acquisition of the series of energy loss images. One is not left with the impression that anything logical is happening that would permit one to arrive at the result of the B-distribution: The images at 178 eV are brighter than the one on the boron edge at 201 eV. This could be due to photographic processing or possibly an automatic gain adjustment of the camera of the microscope. Thus it appears that some magic has occurred to get the result. Please comment.

Authors: We agree that the fact that the reference images recorded at lower energy losses (150 eV, 178 eV - only the latter are presented in the manuscript) are brighter than the boron-specific one (201 eV) might be irritating to the reader. However, by looking at electron energy loss spectra it becomes clear that this is a common situation in most of the cases because of the steep declining of intensity with raising energy losses; e.g., please consider figure 5: though it is not the purpose of this figure, the high intensity of images recorded at an energy loss of 178 eV can easily be estimated by visual extrapolation. The boron signal presented in the figure is, however, clearly distinct from the backgroud curve, which can be easily extrapolated visually.

As explained in the text, in the case of ESI recordings this extrapolation of the background curve is done accurately for each pixel: using two reference images recorded at 150 eV and 178 eV, the well established three-window-method was used to compute the slope of the background curve to be substracted from the values recorded just above the boron edge. Positive differences mean presence of an onset of the curve due to boron presence, no differences mean no signal.

We shortly described the course of electron energy loss spectra in our manuscript and also explained the three-window-method (see Hardware requirements for ESI-Immunocytochemistry).